Shape Effect on Nanoparticle Solvation: A Comparison of Morphometric Thermodynamics and Microscopic Theories

ARTICLE *in* LANGMUIR · APRIL 2012

Impact Factor: 4.46 · DOI: 10.1021/la2051178 · Source: PubMed

3 AUTHORS:

Zhehui Jin
Reservoir Engineering Research Institute
18 PUBLICATIONS **333** CITATIONS
SEE PROFILE

Jehoon Kim
Massachusetts Institute of Technology
9 PUBLICATIONS **19** CITATIONS
SEE PROFILE

Jianzhong Wu
University of California, Riverside
155 PUBLICATIONS **4,328** CITATIONS
SEE PROFILE

Langmuir

Article

pubs.acs.org/Langmuir

Shape Effect on Nanoparticle Solvation: A Comparison of Morphometric Thermodynamics and Microscopic Theories

Zhehui Jin, Jehoon Kim, and Jianzhong Wu*

Department of Chemical and Environmental Engineering and Department of Mathematics, University of California—Riverside, Riverside, California 92521, United States

ABSTRACT: Conventional wisdom for controlling the nanoparticle size and shape during synthesis is that particle growth favors the direction of a facet with the highest surface energy. However, the particle solvation free energy, which dictates the particle stability and growth, depends not only on the surface area and surface free energy but also on other geometric measures such as the solvent excluded volume and the surface curvature and their affiliated thermodynamic properties. In this work, we study the geometrical effects on the solvation free energies of nonspherical nanoparticles using morphometric thermodynamics and density functional theories. For idealized systems that account for only molecular excluded-volume interactions, morphometric thermodynamics yields a reliable solvation free energy when the particle size is significantly larger than the solvent correlation length. However, noticeable deviations can be identified in comparison to the microscopic theories for predicting the solvation free energies of small nanoparticles. This conclusion also holds for predicting the potential of mean force underlying the colloidal "key-and-lock" interactions. Complementary to the microscopic theories, morphometric thermodynamics requires negligible computational cost, therefore making it very appealing for a broad range of practical applications.

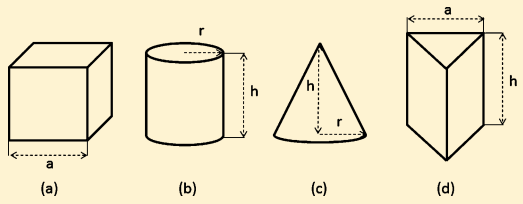

1. INTRODUCTION

The characterization of the local distribution of solvent molecules and the solvation free energy often serves as a starting point for understanding the solution behavior of nanoparticles, including stability and self-assembly. In particular, the solvation free energy is instrumental in controlling the size and shape of nanoparticles during synthesis, and the particle geometry is inextricably related to their unique properties and utilities.[1−3] From a broader perspective, nanoparticle solvation is also important to understanding colloidal forces and the microscopic mechanisms underlying biological processes including protein folding[4] and structure-based rational drug design.[5,6] For a given nanoparticle or a specific conformation of a biomolecule, modern instrumentation and computational methods are now well advanced, enabling the quantification of the solvation free energy and the local solvent structure to the level of atomistic detail. However, these methods are often labor-intensive or computationally demanding and therefore cumbersome for many practical applications. For practical purposes, one often seeks fast yet reliable methods that require little effort or computational cost. Theoretically, a new thrust in that direction is provided by morphological thermodynamics, which describes the solvation free energy in terms of various geometric measures of the solute−solvent interface and the affiliated thermodynamic variables. The geometrical measurements characterize the volume, surface area, integrated mean, and Gaussian curvatures of the space occupied by the solute, and their affiliated thermodynamic quantities are independent of the solute size and geometry.[7] Proposed first by Wagner for microemulsions[8] and then by Mecke, Roth, and co-workers for solvation over the past few years,[7,9,10] the thermogeometric method has been successfully applied to a wide variety of systems, including the solvation of proteins.[11−18]

A cornerstone of morphometric thermodynamics is the Hadwiger theorem from integral geometry concerning the valuations of convex bodies.[19,20] This mathematical theorem asserts that for a functional defined for the set of bodies B in space $\mathbf{R}$ that satisfies motion invariance, conditional continuity, and additivity, the functional can be presented by a bilinear combination of the intrinsic volume of B in different dimensions.[21,22] The Hadwiger theorem suggests that the solvation free energy of a rigid particle is a bilinear function of four geometrical measures (viz., the solute volume, surface area, and integral mean and Gaussian curvatures) and the corresponding thermodynamic coefficients (viz., pressure, surface tension, and bending rigidities, respectively). Although the Hadwiger theorem is not strictly applicable to the solvation free energy if the solute−solvent interaction consists of a long-ranged potential,[7] if the solute size is comparable to the solvent correlation length, or if the solute has a concave shape,[21] it has been shown that the morphometric method predicts the solvation free energy in good agreement with the results from the 3D hypernetted-chain (HNC) equation[10] or from the classical density functional theory (DFT).[14] Recently, the morphological method has been applied to the study of solvation in water[18] and to proteins in multicomponent solvents.[15]

Received: December 27, 2011
Revised: February 23, 2012
Published: April 13, 2012

dx.doi.org/10.1021/la2051178 | *Langmuir* 2012, 28, 6997−7006

The objectives of this work are twofold. First, we use morphological thermodynamics to examine the shape effects on the solvation free energies of nanoparticles that are ignored in conventional interfacial thermodynamics. Because the macroscopic approach is not strictly valid on microscopic length scales, a comparison of the solvation free energies from different theoretical predictions provides insight into the strengths and limits of the morphological method. In addition, we test the performance of the morphological method for predicting colloidal lock-and-key interactions. Specifically, we use the morphometric method to investigate the solvation free energies of four types of idealized nonspherical particles and the depletion potentials in colloidal lock-and-key systems. Unlike that for a spherical particle, the solvation free energy of a nonspherical object depends on the size and the solute−solvent surface geometry. In particular, the edges and vertexes of the nonspherical particles make additional contributions to the solvation free energy. Such effects have not been investigated previously. The particle shape also plays an important role in colloidal lock-and-key interactions that entail colloidal spheres (keys) interacting with spherical cavities (locks).[23]

As in previous applications of the morphometric method,[16,24−26] we consider the solvation of hard particles in a hard-sphere solvent. In other words, we are concerned only with the molecular excluded volume effects of the solute−solvent interactions. Although clearly the hard-sphere model is an oversimplification for any realistic solvent, the system is ideal for testing the numerical performance of the morphometric method and for studying the shape effects of nanoparticle solvation. The hard-sphere model captures at least in part the solvent depletion or the excluded volume effects in realistic systems. For comparison with predictions from microscopic methods, we conduct in parallel theoretical investigations based on the DFT and Monte Carlo (MC) simulations. The DFT methods are selected for comparison because they are numerically more accurate than mean-field theories and provide potential alternatives to simulation methods for the rapid prediction of the solvation free energies.[27] We expect that a comparison of the solvation free energies and the depletion potentials from different theoretical methods may shed light on the future development of analytical solvation models toward industrial-scale engineering applications.

2. THEORETICAL METHODS

A. Morphometric Thermodynamics. As in many previous applications of the morphometric method,[16,24−26] we consider the solvation of nonspherical nanoparticles in a solvent of uniform hard spheres. The athermal system provides a simple yet nontrivial representation of the solvent excluded volume or depletion effects that are relevant to molecular solvation as well as colloidal self-assembly. Throughout this work, the free energy of solvation is defined as the reversible work of inserting a nanoparticle from a fixed position in vacuum into a fixed position in the bulk solvent.

On the basis of the Hadwiger theorem, morphometric thermodynamics[10,19] predicts that the solvation free energy F_{sol} of a nanoparticle, here designated as a continuous convex body $\mathbf{B}$, can be expressed in terms of a bilinear function of four geometrical (Minkowski) measurements and the corresponding thermodynamic coefficients:

$$F_{sol} = PV + \sigma A + \kappa C + \bar{\kappa} X \tag{1}$$

Here, $V(\mathbf{B})$ stands for the excluded volume of the solute particle, $A(\mathbf{B})$ stands for the total solute−solvent interfacial area, $C(\mathbf{B})$ and $X(\mathbf{B})$ are the integral mean and Gaussian curvatures of the solute−solvent interface, respectively. The integral curvatures are defined by surface integrations of the local principal curvatures (χ_1 and χ_2) at the solute−solvent interface:

$$C(\mathbf{B}) = \int_{\partial \mathbf{B}} \frac{1}{2}(\chi_1 + \chi_2)\, dA \tag{2}$$

$$X(\mathbf{B}) = \int_{\partial \mathbf{B}} \chi_1 \chi_2\, dA \tag{3}$$

The coefficients on the right side of eq 1 are familiar thermodynamic variables: the solvent bulk pressure P, the solute−solvent interfacial tension σ at the planar limit, and the surface bending rigidities κ and $\bar{\kappa}$ of the solute−solvent interface. These coefficients are defined by the properties of the pure solvent and by the solute−solvent interactions but are independent of the particle size and geometry (body $\mathbf{B}$).[7]

Equation 1 is exact if the solvation free energy satisfies motion invariance, continuity, and additivity as required by the Hadwiger theorem. Although motion invariance and continuity are automatically satisfied for the solvation free energy, additivity holds exactly only in the thermodynamic limit (i.e., when both the solute and its embedding thermodynamic system are infinitely large). Nevertheless, we expect that additivity remains a good approximation if the solute has a convex shape and its size is much larger than the solvent correlation length. For a solute particle represented by a rigid convex body, the four geometrical measures can be calculated from Steiner's formula.[28]

The thermodynamic coefficients affiliated with the geometric measures can be obtained from experimental, simulation, and theoretical results for the solvation free energies of solutes with relatively simple geometry (e.g., spherical particles of different diameters).[10] Although no thermodynamic coefficients are explicitly related to the solute edges and corners, their influence on the solvation free energy is integrated into the curvature and the corresponding bending energy as shown in the last two terms of eq 1.

For hard particles in a hard-sphere solvent, analytical expressions for the thermodynamic coefficients have been derived on the basis of white bear version II (WBII) of the fundamental measure theory (FMT)[21,29]

$$\frac{\beta P}{\rho_b} = \frac{1 + \eta + \eta^2 - \eta^3}{(1-\eta)^3} \tag{4}$$

$$\frac{\beta\sigma}{\rho_b (d/2)} = -\frac{1 + 2\eta + 8\eta^2 - 5\eta^3}{3(1-\eta)^3} - \frac{\ln(1-\eta)}{3\eta} \tag{5}$$

$$\frac{\beta\kappa}{\rho_b (d/2)^2} = \frac{4 - 10\eta + 20\eta^2 - 8\eta^3}{3(1-\eta)^3} + \frac{4\ln(1-\eta)}{3\eta} \tag{6}$$

$$\frac{\beta\bar{\kappa}}{\rho_b (d/2)^3} = -\frac{4 - 11\eta + 13\eta^2 - 4\eta^3}{3(1-\eta)^3} - \frac{4\ln(1-\eta)}{3\eta} \tag{7}$$

where d is the diameter of a hard-sphere solvent, ρ_b is the number density of the hard-sphere solvent in the bulk, and $\eta = \pi\rho_b d^3/6$ is the solvent packing fraction. As usual, $\beta = 1/(k_B T)$,

dx.doi.org/10.1021/la2051178 | Langmuir 2012, 28, 6997−7006

where k_B is the Boltzmann constant and T is the absolute temperature. For uniform systems, the modified FMT free energy reduced to that from the Carnahan−Staling equation of state.[30] Like the bulk equation of state, FMT[31,32] has been proven to be the most accurate theory for the structural and thermodynamic properties of inhomogeneous hard-sphere fluids.

Whereas the morphometric method has been used before to study protein solvation and interactions between spherical particles,[21] we are unaware of previous work on its application to nanoparticles with nonspherical geometries. To study the effects of particle shape on the solvation free energy, we consider the solvation of four idealized particles: cubes, cylinders, cones, and equilateral triangular prisms (Figure 1).

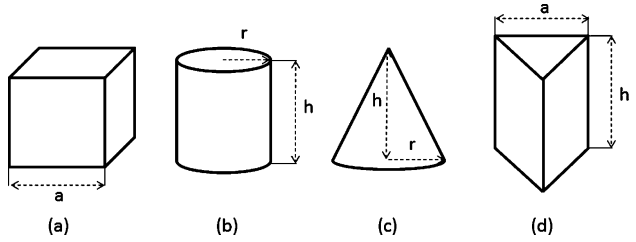

Figure 1. Schematic representation of **B** with the different geometries considered in this work: (a) cube, (b) cylinder, (c) cone, and (d) equilateral triangle prism.

Different from spherical particles, these nanoparticles have sharp edges and vertexes and their contributions to the interfacial properties are not well defined by conventional methods. To validate the predictions of morphometric thermodynamics, we will compare the results with predictions from microscopic approaches including simulation and DFT calculations. Furthermore, we will test the performance of the morphometric method for predicting the colloidal lock-and-key interactions.

B. Density Functional Theory. As an alternative to molecular simulations, DFT provides a generic computational framework for predicting the microscopic structure and thermodynamic properties of macroscopic systems on the basis of the molecular constituents.[33,34] Because DFT is focused on density profiles instead of microstates and provides analytical expressions for thermodynamic variables of interest, it is computationally more efficient than simulation methods. For hard particles in a hard-sphere solvent, the free energies of solvation can be calculated either from the potential distribution theorem[35] or by the direct evaluation of the grand potential.[12] Because the former requires an accurate free-energy functional for the solute−solvent mixture that is not readily available, the latter method is used in this work.

The free energy of solvation predicted by eq 1 can be tested with that from 3D-DFT or from the MC-DFT calculations.[24] MC-DFT refers to a combination of MC simulation for acquiring the 3D density profiles of the solvent with the DFT equations for solvation free-energy calculations. Although MC simulation is readily applicable to calculating the microscopic structure of complex multidimensional systems, the simulation of thermodynamic quantities such as the solvation free energy is extremely time-consuming. However, DFT provides analytical equations between the microscopic structure and the thermodynamic properties, but the computation of the 3D structures is computationally challenging. MC-DFT combines the merits of simulation and DFT methods but avoids their limitations. In both DFT-based methods, the solvation free energy is calculated from the difference between the grand potential $\Omega(\mathbf{B})$ of hard body **B** in a hard-sphere solvent and that of a bulk system of hard spheres with the same volume and solvent chemical potential:

$$F_{sol} = \Omega(\mathbf{B}) - \Omega_b \tag{8}$$

The grand potential of the inhomogeneous system is calculated from a modified FMT[31,32] and that for the bulk hard-sphere system (Ω_b) is calculated from the Carnahan−Starling equation of state.[30]

The two DFT-based methods differ in the way in which we obtain the 3D density distributions of the solvent hard spheres near the nanoparticle solute. In 3D-DFT, the density profiles are calculated by minimizing the grand potential. At equilibrium, the functional derivative of $\Omega[\rho(\mathbf{r})]$ with respect to $\rho(\mathbf{r})$ vanishes, leading to the Euler−Lagrange equation

$$\rho(\mathbf{r}) = \exp\left\{\beta\mu - \frac{\partial\beta F_{ex}}{\partial\rho(\mathbf{r})} - \beta V(\mathbf{r})\right\} \tag{9}$$

where μ is the chemical potential of the bulk hard-sphere system and F_{ex} represents the intrinsic excess Helmholtz energy. For an athermal system, the external potential, $V(\mathbf{r})$, is given by

$$V(\mathbf{r}) = \begin{cases} \infty, \mathbf{r} \in \partial\mathbf{B} \\ 0, \text{otherwise} \end{cases} \tag{10}$$

The Picard-type iterative method[31] was used to solve eq 9. Functional minimization is performed in a cubic box with the nanoparticle placed at the center and with the 3D density profile expressed in Cartesian coordinates.

In MC-DFT, the density profiles of the solvent hard spheres are obtained from grand canonical Monte Carlo (μVT) simulations. Because FMT is very accurate for inhomogeneous hard-sphere systems, we expect these two procedures to yield similar results. However, it is not immediately obvious whether the MC calculation or the 3D minimization has better numerical efficiency. As in functional minimization, we use a cubic simulation box with regular periodic boundary conditions and the nanoparticle fixed in the center of the simulation box. The number of solvent hard spheres in the MC simulation varies with the shape and size of the nanoparticle such that the boundary effects can be neglected. In each MC simulation, we run 1 million MC cycles for equilibration and 5 million cycles to sample the solvent density profiles.

3. RESULTS AND DISCUSSION

We first consider the effects of nanoparticle shape on the solvation free energy based on four types of nonspherical particles (Figure 1) in hard-sphere solvents at different packing fractions. The solvation free energy of each particle depends on the particle size and shape as well as the solvent bulk density. We compare the numerical performance of the morphometric method with 3D-DFT and MC-DFT calculations. In addition, we apply the morphometric approach to a colloidal lock-and-key system and compare the colloidal forces with the results from microscopic methods.

A. Cubic Particles. The solvation free energy of a cube in a hard-sphere solvent depends only on the edge length (a) and

dx.doi.org/10.1021/la2051178 | Langmuir 2012, 28, 6997−7006

the solvent packing fraction. According to Steiner's formula,[28] the four geometric measures of the cube are given by

$$\begin{cases} V = a^3 \\ A = 6a^2 \\ C = 3\pi a \\ X = 4\pi \end{cases} \quad (11)$$

In the 3D-DFT and MC-DFT calculations, the center of mass of the cube is placed at the origin $(x, y, z) = (0, 0, 0)$ and the simulation box is also cubic with sides $L_x = L_y = L_z = 12d$ such that the boundary effect can be neglected.

Figure 2 presents the solvation free energy versus edge length a at different solvent densities. The solid line is predicted by morphometric thermodynamics, and the symbols are from 3D-DFT and MC-DFT. At a given solvent density, the solvation free energy increases monotonically with the particle size because of the fact that it takes more work to insert a larger nanoparticle. The solvation free energy also increases with the solvent density. As expected, the results from 3D-DFT and MC-DFT are almost indistinguishable. For the solvation of cubic particles, the agreement between the morphometric and DFT methods is very good in all cases. The excellent agreement among different methods is in part due to the use of Cartesian coordinates that match perfectly with the edges of cubic particles. In other words, for this particular system we can calculate the 3D density profiles and subsequently the solvation free energy in 3D-DFT and MC-DFT very accurately. Although the computational cost for the morphometric method is negligible, it takes several hours or even days to obtain the density profiles from 3D-DFT or MC-DFT (on a single core of an AMD Budapest 2.3 GHz processor computer at the National Energy Research Scientific Computing Center). In particular, MC simulation becomes very time-consuming at high solvent densities.

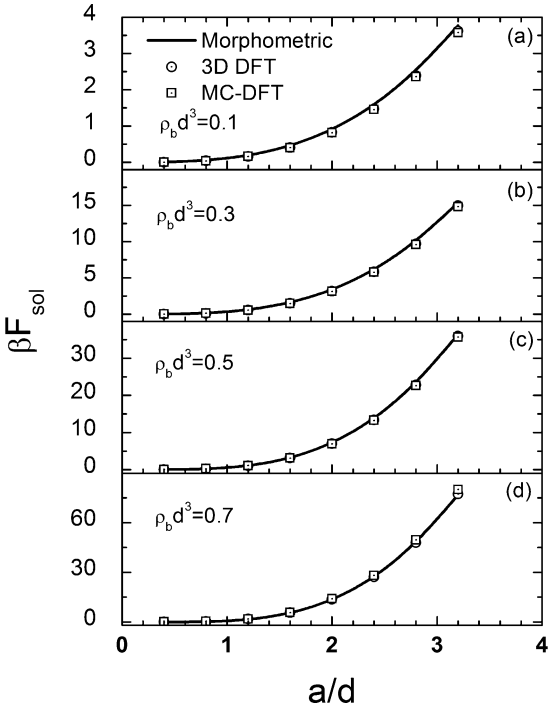

Figure 2. (a) Solvation free energy of cubic **B** vs length a in a hard-sphere solution with solvent density of $\rho d^3 = 0.1$. (b) The same as for part a except that $\rho d^3 = 0.3$. (c) The same as for part a except that $\rho d^3 = 0.5$. (d) The same as for part a except that $\rho d^3 = 0.7$.

B. Cylindrical Particles. For a cylindrical particle of height h and base radius r, the four geometric measures are given by

$$\begin{cases} V = \pi r^2 h \\ A = 2\pi r^2 + 2\pi r h \\ C = \pi h + \pi^2 r \\ X = 4\pi \end{cases} \quad (12)$$

To minimize the number of parameters, we fix the cylinder height at $h = 2d$ for simplicity. As for the cubic case, the center of mass of the cylinder is placed at $(x, y, z) = (0, 0, 0)$ and the simulation box is cubic with sides of $L_x = L_y = L_z = 12d$ in both the MC simulation and DFT calculations.

Figure 3 shows the solvation free energy of a cylindrical particle versus base radius r. Similar to that for a cubic particle, the solvation free energy increases monotonically with the radius at a given solvent density. Overall, the results from the morphometric method are in good agreement with those from the DFT calculations. Because the solvent densities are highly localized near the edges of a cylindrical particle, we attribute the increased discrepancy for large particles dissolved at high solvent density to the Cartesian coordinates used in the DFT calculations. The particle geometry does not perfectly match the grids for the MC sampling of the solvent density profiles.

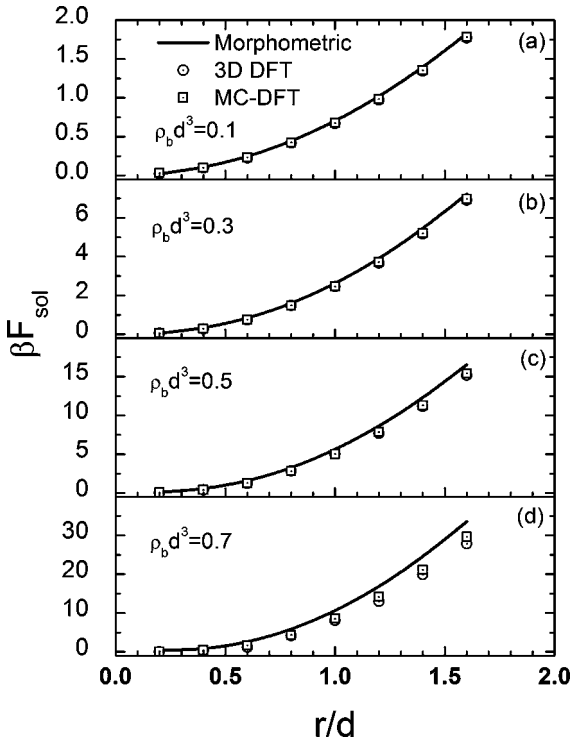

Figure 3. (a) Solvation free energy of a cylinder **B** with height $h = 2d$ vs radius r in a hard-sphere solution with a solvent density of $\rho d^3 = 0.1$. (b) The same as for part a except that $\rho d^3 = 0.3$. (c) The same as for part a except that $\rho d^3 = 0.5$. (d) The same as for part a except that $\rho d^3 = 0.7$.

C. Cones. The four geometric measures of a right circular cone are given by

dx.doi.org/10.1021/la2051178 | Langmuir 2012, 28, 6997−7006

$$\begin{cases} V = \dfrac{\pi}{3} r^2 h \\ A = \pi r^2 \left(1 + \dfrac{\sqrt{h^2 + r^2}}{r}\right) \\ C = \pi r \left(\dfrac{\pi}{2} + \arctan\left(\dfrac{r}{h}\right) + \dfrac{h}{r}\right) \\ X = 4\pi \end{cases} \quad (13)$$

where r is the base radius and h is the height. As for a cylinder, we fix the height at $h = 2d$. In 3D-DFT and MC-DFT calculations, the origin of the coordinates $(x, y, z) = (0, 0, 0)$ is placed halfway up the cone. The simulation box is again cubic with sides of $L_x = L_y = L_z = 12d$.

Figure 4 presents the size dependence of the solvation free energies of hard cones dissolved in a hard-sphere solvent at different solvent densities. Similar to other nanoparticles, in most cases the solvation free energy predicted by the morphometric method agrees well with 3D-DFT and MC-DFT. However, at high solvent density ($\rho d^3 = 0.7$), the morphometric method predicts that the solvation free energy exhibits a minimum for a cone of moderate size whereas both the 3D-DFT and MC-DFT predictions show a monotonic increase in the free energy as the particle grows. The discrepancy at small particle size is probably due to the correlation effect that becomes stronger and longer-ranged at higher solvent density. In other words, the performance of the morphometric method deteriorates when the cone size is comparable to the correlation length. In contrast to the case for cylindrical nanoparticles, the agreement between the DFT and morphometric methods improves as the particle base radius increases.

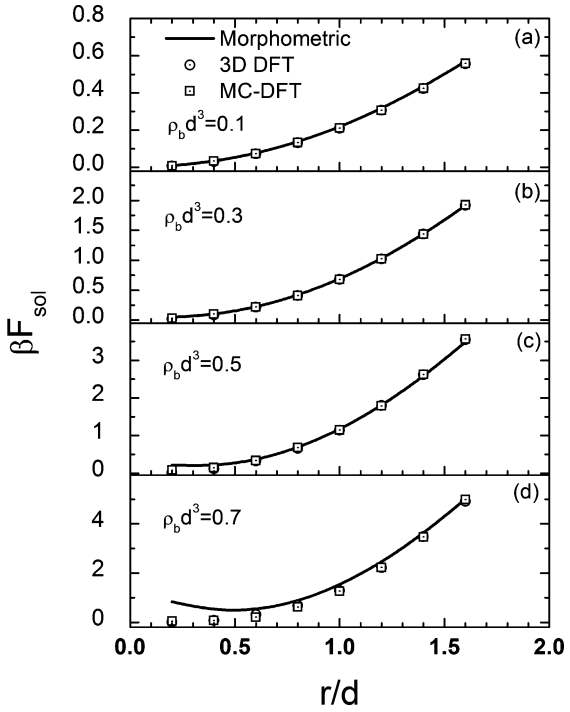

Figure 4. (a) Solvation free energy of a cone **B** of height $h = 2d$ vs radius r in a hard sphere solution with solvent density $\rho d^3 = 0.1$. (b) The same as for part a except that $\rho d^3 = 0.3$. (c) The same as for part a except that $\rho d^3 = 0.5$. (d) The same as for part a except that $\rho d^3 = 0.7$.

D. Equilateral Triangle Prisms. We now consider the solvation of equilateral triangle prisms in a hard-sphere solvent. For simplicity, the prism height is fixed at $h = 2d$, and a stands for the triangular side length. The four geometric measurements of an equilateral triangle prism are given by

$$\begin{cases} V = \dfrac{\sqrt{3}}{4} a^2 h \\ A = \dfrac{\sqrt{3}}{2} a^2 + 3ah \\ C = \pi h + \dfrac{3}{2}\pi a \\ X = 4\pi \end{cases} \quad (14)$$

In 3D-DFT and MC-DFT calculations, the center of mass of the equilateral triangle prism is placed at $(x, y, z) = (0, 0, 0)$ and the box is cubic with sides of $L_x = L_y = L_z = 12d$.

Figure 5 shows the solvation free energies calculated from the morphometric method and DFT methods. Here, the 3D-DFT and MC-DFT results were depicted together for easy comparison. Similar to the cylinder case, there is a discrepancy between the morphometric approach and the DFT methods for large prisms dissolved in a high-density solvent. The discrepancy grows as the bulk solvent density increases. Meanwhile, the results from 3D-DFT and MC-DFT are slightly different because the grids of Cartesian coordinates cannot match a perfect triangle prism. At high bulk solvent

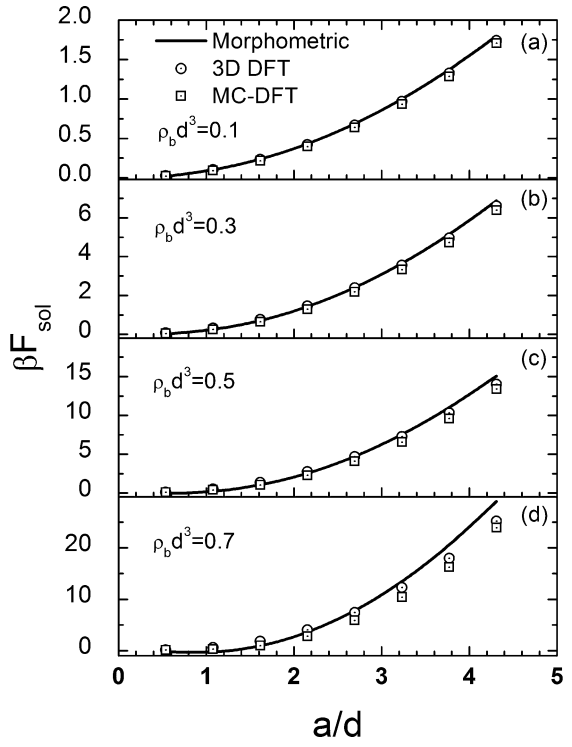

Figure 5. (a) Solvation free energy of an equilateral triangular prism **B** of height $h = 2d$ in a hard-sphere solution with solvent density $\rho d^3 = 0.1$. (b) The same as for part a except that $\rho d^3 = 0.3$. (c) The same as for part a except that $\rho d^3 = 0.5$. (d) The same as for part a except that $\rho d^3 = 0.7$.

dx.doi.org/10.1021/la2051178 | Langmuir 2012, 28, 6997−7006

density, the morphometric method erroneously predicts that the solvation free energy is negative when the side length a is small, which contradicts the results from 3D-DFT and MC-DFT. The negative solvation energy indicates that the morphometric approach breaks down because the solvent correlation length is comparable to the particle size.

E. Comparison between Particles of Different Geometries. A study of nanoparticles with the same volume and surface area but different geometries allows us to examine the effects of particle shape on the solvation free energy. For convex nanoparticles, the integral Gaussian curvature is invariant with particle geometry. As a result, when the particle volume and surface area are fixed, the shape effect is manifested exclusively in terms of the contribution from the integral mean curvature to the total solvation free energy.

Figure 6a compares the solvation free energies of cylinders relative to that of a cube with the same solvent excluded volume V and surface area A. For a given cube of edge length a, there are two types of cylinders that give the same V and A: type 1 has radius $r/a = 0.401$ and height $h/a = 1.982$; type 2 has radius $r/a = 0.713$ and height $h/a = 0.626$. The difference in the solvation free energy is reflected in the curvature contribution:

$$\kappa\Delta C(a) = \kappa[C^{\text{solute}}(a) - C^{\text{cubic}}(a)] \quad (15)$$

The cone and equilateral triangle prism are not compared here because particles with these shapes cannot have the same volume and surface area as those of a cube. Figure 6a indicates that the integral mean curvature contributions in cylinder types 1 and 2 are quite different. Although the relative solvation free energy of the type 1 cylinder (longer and thinner) is positive, the opposite is true for the type 2 cylinder (shorter and thicker). In other words, the solvation free energy is decreased when the radius and height of the cylinder are close to each other. It should be noted that the surface of a cube is not curved according to conventional interfacial thermodynamics, but because of the edge effect, its solvation energy can be either larger or smaller than that of a cylinder depending on the aspect ratio.

For comparison, Figure 6a also shows the relative solvation free energy of a sphere with the same V or A as that of a cube. In both cases, the solvation free energy of a sphere is lower than that of either cylinder 1 or 2. In comparison to that for a cube of either the same V or the same A, the relative curvature contribution is always negative. At the same V, a sphere has less surface area than a cube ($A_{\text{sphere}}/A_{\text{cube}} = 0.81$), whereas at the same A a sphere has a larger volume ($V_{\text{sphere}}/V_{\text{cube}} = 1.38$). In contrast to the case of the same volume, a sphere with the same area has a larger solvation free energy because of a stronger contribution from the excluded volume effect. In both cases, the effect of curvature on the solvation free energy is relatively insignificant.

Figure 6b presents the solvation free energies of a cylinder and an equilateral triangle prism relative to that of a cone with equal radius and height ($h_0 = r_0$). Similar to Figure 6a, these particles have the same solvent excluded volume and surface area. For a given cone dimension, there are two types of cylinders and two types of equilateral triangle prisms that give identical volumes and surface areas: cylinder type 1 has radius $r/r_0 = 0.298$ and height $h/h_0 = 3.751$; cylinder type 2 has radius $r/r_0 = 0.919$ and height $h/h_0 = 0.395$; equilateral triangle prism type 1 has edge length $a/r_0 = 2.24$ and height $h/h_0 = 0.482$; and equilateral triangle prism type 2 has edge length $a/r_0 = 1.115$ and height $h/h_0 = 1.946$. Although both equilateral triangle prisms have higher solvation free energies in comparison to the cone, cylinder type 2 has a lower solvation free energy and the opposite is true for cylinder type 1. A comparison between the solvation free energies of prism and cone particles indicates that edges and corners make additional contributions to the solvation free energy. As depicted in Figure 6a, the shorter and thicker cylinder (type 2) has a smaller solvation free energy. In other words, a reduction of the size disparity

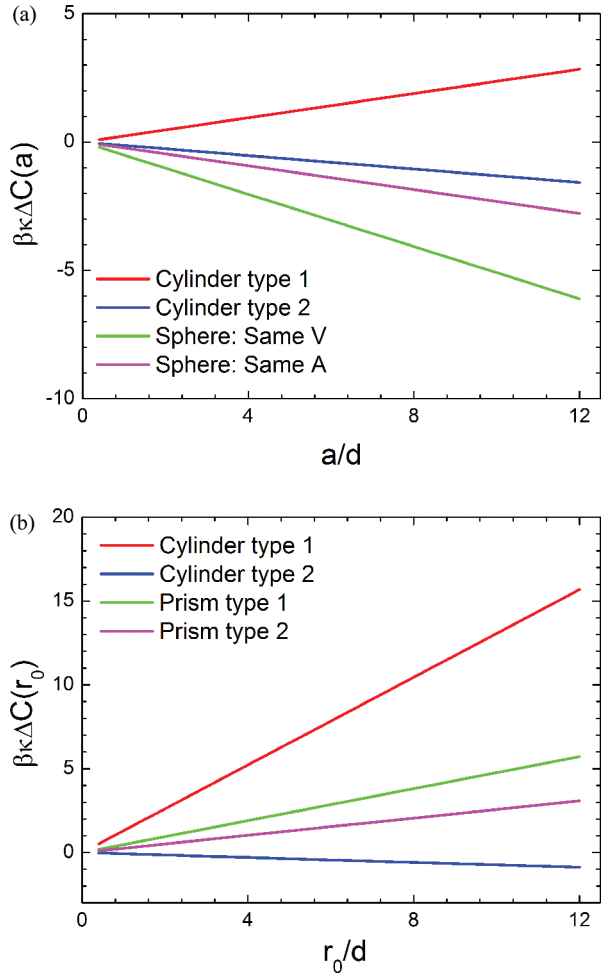

Figure 6. (a) Relative curvature contribution with respect to a cube with edge length a, $\kappa\Delta C(a) = \kappa[C^{\text{solute}}(a) - C^{\text{cubic}}(a)]$, of cylinders with the same volumes and surface areas as those of the same cube immersed in a hard-sphere solution with a bulk density of $\rho d^3 = 0.7$. The red line indicates a type 1 cylinder with radius $r/a = 0.401$ and height $h/a = 1.982$, and the blue line indicates the type 2 cylinder with radius $r/a = 0.713$ and height $h/a = 0.626$. The green line presents the relative curvature contribution of spheres with the same volume as the cube with edge length a, and the magenta line depicts that of a sphere with the same surface areas as a cube with edge length a. The radius of the sphere is $r/a = 0.62$ for the same V and $r/a = 0.69$ for the same A. (b) Relative curvature contribution with respect to a cone with radius r_0 and height $h_0 = r_0$; $\kappa\Delta C(r_0) = \kappa[C^{\text{solute}}(r_0) - C^{\text{cone}}(r_0)]$ of a cylinder and equilateral triangle prism with the same volume and surface area as that of the same cone immersed in a hard-sphere solution with bulk density $\rho d^3 = 0.7$. The red line indicates cylinder type 1 with radius $r/r_0 = 0.298$ and height $h/h_0 = 3.751$, the blue line indicates cylinder type 2 with radius $r/r_0 = 0.919$ and height $h/h_0 = 0.395$, the green line presents equilateral triangle prism type 1 with edge length $a/r_0 = 2.24$ and height $h/h_0 = 0.482$, the blue line indicates equilateral triangle prism type 2 with edge length $a/r_0 = 1.115$ and height $h/h_0 = 1.946$.

dx.doi.org/10.1021/la2051178 | Langmuir 2012, 28, 6997−7006

between the radius/edge and height lowers the solvation free energy for both the cylinder and equilateral triangle prism.

F. Lock-and-Key System in a Hard-Sphere Solvent. The colloidal lock-and-key system considered in this work consists of a planar lock with a hemispherical cavity and a key represented by a spherical particle. Both the lock and the key are immersed in a hard-sphere solvent. The colloidal lock-and-key system has been studied before with 3D integral-equation theory,[16] the curvature expansion method,[25] the hybrid MC-DFT method,[24] the level-set method with the variational implicit solvent model,[36,37] and computer simulations.[38] In this work, we re-examine the potential of mean force (PMF) for the lock-and-key interactions using the morphological thermodynamics.

As discussed in ref 24, we consider only the perpendicular alignment of the lock and key particles. Figure 7 shows a schematic representation of the lock and key system. The center of the hemispherical cavity is placed at $(x_0, 0, 0)$, and the center of the key is located at $(x, 0, 0)$ with varying x. The radius of the cavity is fixed at $R_{lock} = 2.5d$. We examine the depletion potential $W(x-x_0)$ for various key particles with radius R_{key} along the symmetric axis.

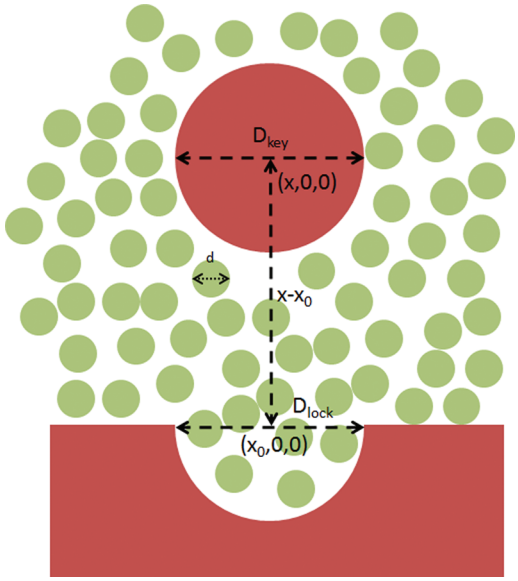

Figure 7. The schematic representation of the lock and key system. The key is a large spherical particle with diameter D_{key}, and the lock is a substrate with a hemispherical pocket with diameter D_{lock}. The separation between the key and lock is represented by the distance between the center of the key at $(x, 0, 0)$ and the lock at $(x_0, 0, 0)$.

When the key and lock particles are aligned, the PMF depends only on the center-to-center distance r between the hemispherical cavity and the spherical key

$$W(r) = \Omega(r) - \Omega(\infty) \tag{16}$$

where $\Omega(r)$ is the grand potential of the system with lock and key separated by a distance r and $\Omega(\infty)$ is that of the same system with particles that are far apart (i.e., $r \to \infty$). Substituting eq 8 into eq 16 gives

$$W(r) = F_{sol}(r) - F_{sol}(\infty) \tag{17}$$

where $F_{sol}(r)$ is the solvation free energy of the entire lock-and-key system when the particles are separated by a distance r and $F_{sol}(\infty)$ is that of the same system with particles that are far apart. When the lock and key are far apart, the lock-and-key particles are not correlated. As a result, $F_{sol}(\infty)$ can be separated into the solvation free energies of the lock F_{sol}^{lock} and that of the key F_{sol}^{key}:

$$F_{sol}(\infty) = F_{sol}^{lock} + F_{sol}^{key} \tag{18}$$

As for the solvation of nanoparticles, both the morphometric and DFT methods are used to study the solvation free energies of the lock, the key, and the lock-and-key complexes.

The geometric measurements of the spherical key particle are known exactly,

$$\begin{cases} V = \frac{4}{3}\pi\left(R_{key} + \frac{d}{2}\right)^3 \\ A = 4\pi\left(R_{key} + \frac{d}{2}\right)^2 \\ C = 4\pi\left(R_{key} + \frac{d}{2}\right) \\ X = 4\pi \end{cases} \tag{19}$$

The geometric measurements of a substrate with a semi-spherical cavity of radius R_{lock} at the surface of a cylinder with radius R_T and height h (see Figure 8) are given by

$$\begin{cases} V = \frac{\pi d}{2}(R_T^2 - R_{lock}^2) + \pi R_{lock}^2 d - \frac{\pi}{2}R_{lock}d^2 \\ \quad + \frac{\pi^2}{8}R_{lock}d^2 + \pi R_T^2 h - \frac{2\pi}{3}R_{lock}^3 \\ A = 2\pi R_{lock}^2 - 2\pi R_{lock}d + \pi(R_T^2 - R_{lock}^2) \\ \quad + \frac{\pi^2}{2}R_{lock}d + \pi R_T^2 \\ C = -2\pi R_{lock} + \frac{\pi^2}{2}R_{lock} \\ X = 0 \end{cases} \tag{20}$$

To obtain the four geometric measurements of the entire lock-and-key system, we create a contour parallel to the solvent-accessible surface of the solute with distance u. Figure 8 shows the effective shapes of the lock, the key, and the lock-and-key complexes. At a given key and lock separation, we numerically calculate the volume $V(u)$ enclosed by such surfaces and subsequently the surface area $A(u)$, integral mean curvature $C(u)$, and integral Gaussian curvature $X(u)$ from[14]

$$\begin{aligned} A(u) &= -\partial_u V(u) \\ C(u) &= -\frac{1}{2}\partial_u A(u) \\ X(u) &= -\partial_u C(u) \end{aligned} \tag{21}$$

The desired geometric measurements of the lock-and-key complex are obtained in the limit of $u \to 0$ by solving $V(u)$ numerically.

Figures 9a and 9b present the depletion potential between the lock and key particles when the key is slightly smaller than the lock cavity and when there is a perfect match of the lock size, respectively. The results calculated from morphological thermodynamics are compared with the two DFT-based methods and with direct MC simulations.[24] Because an

dx.doi.org/10.1021/la2051178 | Langmuir 2012, 28, 6997−7006

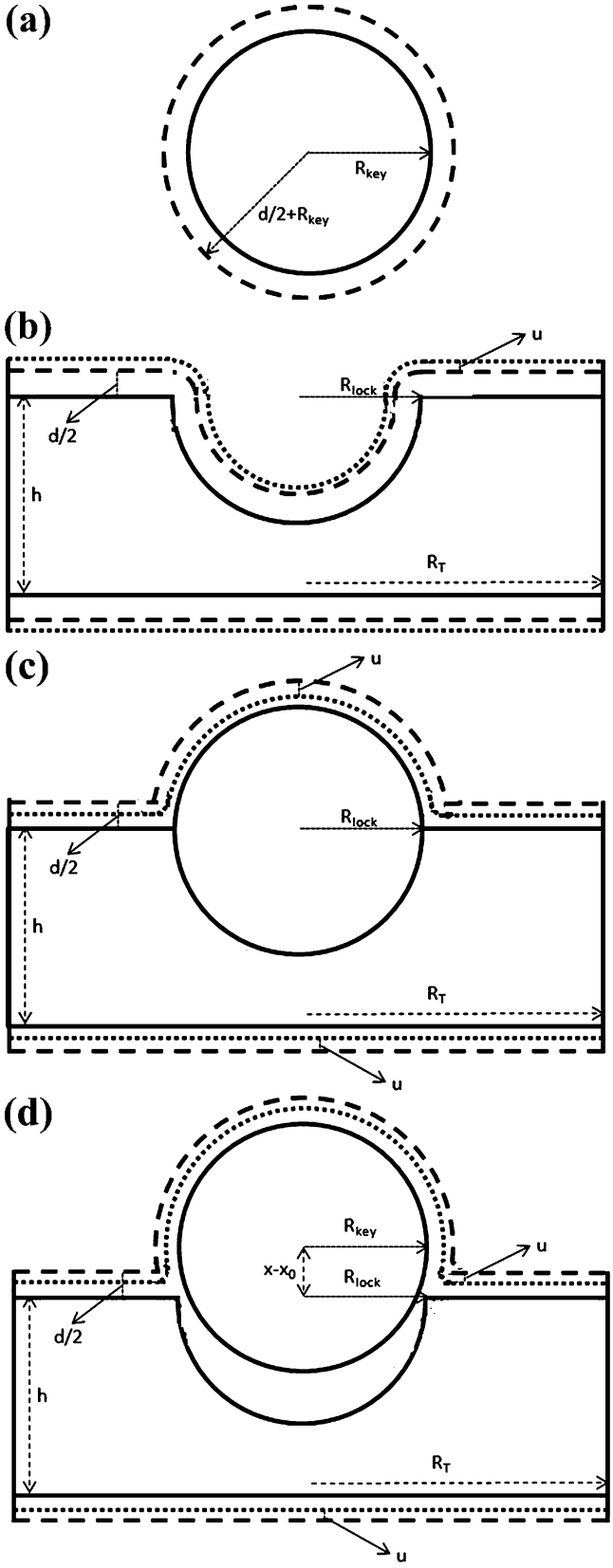

Figure 8. (a) Schematic representation of the key particle with radius R_{key}. The dashed line shows the solvent-accessible surface enclosing the excluded volume of the key particle. (b) The same for part a except for the lock particle. (c) The same as for part a except for the lock-and-key complex with the radius of the key particle $R_{key} = R_{lock}$ located at (x_0, 0, 0) where the dotted line represents a surface parallel to the solvent-accessible surface at a distance u. (d) The same as for part c except for the lock-and-key complex with a radius of key particles $R_{key} = R_{lock}$ located at (x, 0, 0).

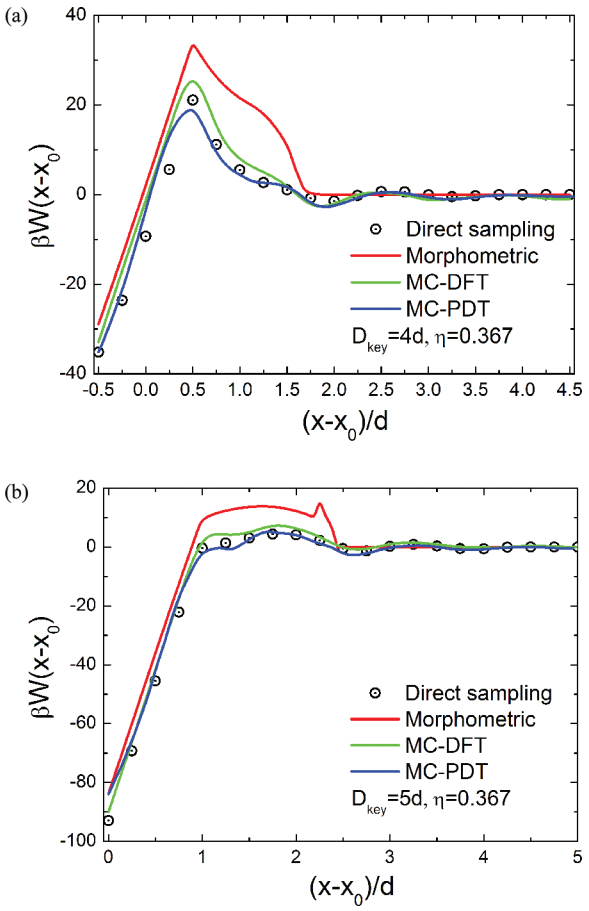

Figure 9. (a) Depletion potential between a hard spherical key with key diameter $D_{key} = 4d$ and a hard hemispherical lock substrate with lock diameter $D_{lock} = 5d$ in a hard-sphere solvent at a bulk packing fraction of $\eta = 0.367$. We compare the morphological thermodynamics (red line) with the MC-DFT (green line) and MC-PDT (blue line) methods and the simulation data (symbols) reported in ref 24. (b) The same as for part a except with key diameter $D_{key} = 5d$.

analytical expression is available for the free-energy functional of the hard-sphere mixture, we may obtain the potential of mean force from the potential distribution theorem (PDT).[39] In this method, we first obtain the solvent density profile near the lock particle, and the lock-and-key potential is calculated from the local excess chemical potential of the key particle. The solvent density profile can be obtained either from MC simulation or from DFT. The former is referred to as MC-PDT, and the latter is referred to as DFT-PDT. More details about the PDT calculations can be given in ref 24. Alternatively, the potential of mean force can be obtained from the integration of mean force that is directly sampled from MC simulation for two particles at a certain separation.

In comparison with MC simulations, the morphometric method is not as accurate as MC-DFT and MC-PDT for predicting the depletion potential.[24] When the separation ($x - x_0$) is larger than the solvent diameter, a cavity appears in the interior of the lock-and-key complex. In this case, the Hadwiger theorem is not valid. The results from morphological

dx.doi.org/10.1021/la2051178 | Langmuir 2012, 28, 6997−7006

thermodynamics show a curve-up shape for a smaller key (R_{key} = 2d) and a sudden jump if there is a perfect match (R_{key} = 2.5d, near x = 2.15d). The unphysical jump arises from the contribution from the mean integral curvature, similar to that appearing in sphere−sphere interactions.[14] Furthermore, morphological thermodynamics predicts that the lock-and-key particles do not affect each other when their excluded volumes are completely separated. However, the density correlation makes additional contributions to the solvent-mediated interactions. When the Hadwiger theorem is not valid, morphological thermodynamics predicts a qualitatively inaccurate potential of mean force in comparison to MC simulation and DFT calculations.

Nevertheless, Figure 9 shows that the morphometric thermodynamics captures the potential of mean force at least semiquantitatively for both cases when x is less than one diameter of the hard-sphere solvent. The numerical deficiency probably occurs because the size of the concave container is comparable to the correlation length of the solvent. If the concave size is much larger than the correlation length, then we expect that the morphological thermodynamics will agree better with the simulation results.[7] Indeed, the morphological approach shows satisfactory agreement with simulation even when the concave size is comparable to the correlation length.

4. SUMMARY

In this work, we used morphometric thermodynamics to study the solvation free energies of nonspherical nanoparticles and colloidal lock-and-key interactions in a hard-sphere solvent. In comparison to molecular simulation and microscopic methods such as classical density functional theory (DFT), the morphological method does not require the configurations of the solvent molecules, thus it drastically reduces the computational cost. Although the statistical-mechanical methods perform best on small length scales, the morphological thermodynamics does not scale with the system size but becomes most accurate on large scales. As a result, the two approaches are complementary to each other and a combination of both can be most profitable for practical applications.

Ideas similar to the morphometric method have been deployed in an extension of the scaled-particle theory in studying hydrophobic solvation.[40] In the application of the morphometric method to particle solvation in realistic solvents (e.g., a Lennard-Jones fluid or water), the thermodynamic coefficients can be obtained from the solvation free energies of spherical particles. Because the thermodynamic properties of the solvent and the solute−solvent interactions are independent of the particle shape, the same coefficients are applicable to particles of arbitrary geometry. Different from that in a hard-sphere solvent, the solvation of nonattractive particles in a realistic solvent may induce drying on the surface when the solvent is in the proximity of saturation. In that case, the additivity condition required by the Hadwiger theorem breaks down and the morphometric thermodynamics becomes inaccurate. The additivity also breaks down on small scales and under conditions where there exist significant long-range correlations and fluctuation effects. Another drawback of the macroscopic approach is that it is not able to account for surface heterogeneity or defects that do not simply scale with the system size. Under those conditions, we must use molecular simulation or microscopic theories. Because morphometric thermodynamics divorces the solute geometry from the thermodynamic properties, this method is powerful in particular for the calculation of the interfacial free energies of continuous systems that adopt different sizes and shapes.

The morphometric thermodynamics compares well with DFT for predicting the solvation free energies of nonspherical particles, viz., a cube, cylinder, cone, and equilateral prism in a hard-sphere solvent with varying bulk density. Although conventional wisdom is that the stability or solvation free energy of a nanoparticle is determined by the solvent excluded volume and surface area, morphological thermodynamics accounts for additional effects due to the surface curvature. For particles with different geometries but the same excluded volume and surface area, the morphological thermodynamics predicts that a reduction of the ratio between the radius/edge and height of the particle lowers the solvation free energy. The DFT calculations also indicate that the solute curvature can have significant effects on the solvent behavior near the solute and subsequently the solvation free energy. In morphometric thermodynamics, the edge and corner effects are taken into account through the integrated curvatures, which make additional contributions to the solvation free energy.[41]

We further applied morphological thermodynamics to the study of the more complicated lock-and-key model system, which includes complex convex and concave geometry. Although the Hadwiger theorem breaks down for solute particles with concave regions that introduce a confinement effect on the solvent, the prediction from morphological thermodynamics is generally good compared to alternative analytical methods and computer simulations. As the concave size increases and confinement effect becomes less significant, the morphometric approach should agree better with computer simulation whereas it costs virtually no extra time. One very attractive feature of the morphometric approach is that it can be easily altered to study solvation in different solvents because the properties of the solvent are presented only by four thermodynamic coefficients.[14]

■ AUTHOR INFORMATION

Corresponding Author

*E-mail: jwu@engr.ucr.edu.

Notes

The authors declare no competing financial interest.

■ ACKNOWLEDGMENTS

We are grateful to the U.S. Department of Energy (DE-FG02-06ER46296) for financial support. This work utilized supercomputers from the National Energy Research Scientific Computing Center (NERSC).

■ REFERENCES

(1) Yin, Y.; Alivisatos, A. P. Colloidal nanocrystal synthesis and the organic-inorganic interface. *Nature* **2005**, *437*, 664.

(2) Chiu, C. Y.; Li, Y. J.; Ruan, L. Y.; Ye, X. C.; Murray, C. B.; Huang, Y. Platinum nanocrystals selectively shaped using facet-specific peptide sequences. *Nat. Chem.* **2011**, *3*, 393.

(3) Burda, C.; Chen, X. B.; Narayanan, R.; El-Sayed, M. A. Chemistry and properties of nanocrystals of different shapes. *Chem. Rev.* **2005**, *105*, 1025.

(4) Eisenberg, D.; McLachlan, A. D. Solvation energy in protein folding and binding. *Nature* **1986**, *319*, 199.

(5) Terry, P, L. Ligand−protein docking and rational drug design. *Curr. Opin. Struct. Biol.* **1995**, *5*, 224.

(6) Marcus, Y. Effect of ions on the structure of water: structure making and breaking. *Chem. Rev.* **2009**, *109*, 1346.
(7) König, P. M.; Roth, R.; Mecke, K. R. Morphological thermodynamics of fluids: shape dependence of free energies. *Phys. Rev. Lett.* **2004**, *93*, 160601.
(8) Wagner, H. Morphological thermodynamics of microemulsions. *Ber. Bunsen-Ges.* **1996**, *100*, 296.
(9) Hansen-Goos, H.; Roth, R.; Mecke, K.; Dietrich, S. Solvation of proteins: linking thermodynamics to geometry. *Phys. Rev. Lett.* **2007**, *99*, 128101.
(10) Roth, R.; Harano, Y.; Kinoshita, M. Morphometric approach to the solvation free energy of complex molecules. *Phys. Rev. Lett.* **2006**, *97*, 078101.
(11) Wu, J. Solvation of a spherical cavity in simple liquids: Stretching the limits. *J. Phys. Chem. B* **2009**, *113*, 6813.
(12) Roth, R.; Evans, R.; Dietrich, S. Depletion potential in hard-sphere mixtures: theory and applications. *Phys. Rev. E* **2000**, *62*, 5360.
(13) Roth, R.; Evans, R. The depletion potential in non-additive hard-sphere mixtures. *Europhys. Lett.* **2001**, *53*, 271.
(14) Oettel, M.; Hansen-Goos, H.; Bryk, P.; Roth, R. Depletion interaction of two spheres-full density functional theory vs. morphometric results. *Eur. Phys. Lett.* **2009**, *85*, 36003.
(15) Kodama, R.; Roth, R.; Harano, Y.; Kinoshita, M. Morphometric approach to thermodynamic quantities of solvation of complex molecules: extension to multicomponent solvent. *J. Chem. Phys.* **2011**, *135*, 045103.
(16) Kinoshita, M.; Oguni, T. Depletion effects on the lock and key steric interactions between macromolecules. *Chem. Phys. Lett.* **2002**, *351*, 79.
(17) Kinoshita, M. Spatial distribution of a depletion potential between a big solute of arbitrary geometry and a big sphere immersed in small spheres. *J. Chem. Phys.* **2002**, *116*, 3493.
(18) Dzubiella, J. How interface geometry dictates water's thermodynamic signature in hydrophobic association. *J. Stat. Phys.* **2011**, *145*, 227.
(19) Mecke, K. R. Integral geometry in statistical physics. *Int. J. Mod. Phys. B* **1998**, *12*, 861.
(20) Hadwiger, H. *Vorlesungen über Inhalt, Oberfläche und Isoperimetrie*: Springer: Berlin, 1957.
(21) Hansen-Goos, H. Ph.D. Thesis, University of Stuttgart, 2008.
(22) Chen, B. A simplified elementary proof of Hadwiger's volume theorem. *Geometriae Dedicata* **2004**, *105*, 107.
(23) Sacanna, S.; Irvine, W. T. M.; Chaikin, P. M.; Pine, D. J. Lock and key colloids. *Nature* **2010**, *464*, 575.
(24) Jin, Z.; Wu, J. Hybrid MC−DFT method for studying multidimensional entropic forces. *J. Phys. Chem. B* **2011**, *115*, 1450.
(25) König, P. M.; Roth, R.; Dietrich, S. Lock and key model system. *Eur. Phys. Lett.* **2008**, *84*, 68006.
(26) König, P. M.; Roth, R.; Dietrich, S. Depletion forces between nonspherical objects. *Phys. Rev. E* **2006**, *74*, 041404.
(27) Zhao, S.; Jin, Z.; Wu, J. New theoretical method for rapid prediction of solvation free energy in water. *J. Phys. Chem. B* **2011**, *115*, 6971.
(28) Mecke, K. R.; Buchert, T.; Wagner, H. Robust morphological measures for large-scale structure in the universe. *Astron. Astrophys.* **1994**, *288*, 697.
(29) Hendrik, H.-G.; Roland, R. Density functional theory for hard-sphere mixtures: the white bear version mark II. *J. Phys.: Condens. Matter* **2006**, *18*, 8413.
(30) Carnahan, N. F.; Starling, K. E. Equation of state for nonattracting rigid spheres. *J. Chem. Phys.* **1969**, *51*, 635.
(31) Yu, Y.-X.; Wu, J. Structures of hard-sphere fluids from a modified fundamental-measure theory. *J. Chem. Phys.* **2002**, *117*, 10156.
(32) Roth, R.; Evans, R.; Lang, A.; Kahl, G. Fundamental measure theory for hard-sphere mixtures revisited: the white bear version. *J. Phys.: Condens. Matter* **2002**, *14*, 12063.
(33) Evans, R. In *Fundamentals of Inhomogeneous Fluids*; Henderson, D., Ed.; Marcel Dekker: New York, 1992; p 85.
(34) Wu, J. Z.; Li, Z. D. Density functional theory for complex fluids. *Int. J. Eng. Educ.* **2007**, *58*, 85.
(35) Henderson, J. R. Potential-distribution theorem mechanical stability and Kirkwood integral-equation. *Mol. Phys.* **1983**, *48*, 715.
(36) Setny, P.; Wang, Z.; Cheng, L. T.; Li, B.; McCammon, J. A.; Dzubiella, J. Dewetting-controlled binding of ligands to hydrophobic pockets. *Phys. Rev. Lett.* **2009**, *103*, 187801.
(37) Cheng, L.-T.; Wang, Z.; Setny, P.; Dzubiella, J.; Li, B.; McCammon, J. A. Interfaces and hydrophobic interactions in receptor-ligand systems: a level-set variational implicit solvent approach. *J. Chem. Phys.* **2009**, *131*, 144102.
(38) Odriozola, G.; Jimenez-Angeles, F.; Lozada-Cassou, M. Entropy driven key-lock assembly. *J. Chem. Phys.* **2008**, *129*, 111101.
(39) Widom, B. Potential-distribution theory and the statistical-mechanics of fluids. *J. Phys. Chem.* **1982**, *86*, 869.
(40) Ashbaugh, H. S.; Pratt, L. R. Colloquium: scaled particle theory and the length scales of hydrophobicity. *Rev. Mod. Phys.* **2006**, *78*, 159.
(41) Marmur, A.; Krasovitski, B. Line tension on curved surfaces: liquid drops on solid micro- and nanospheres. *Langmuir* **2002**, *18*, 8919.